ACS APPLIED ENERGY MATERIALS

www.acsaem.org Article

Solution-Grown Phosphorus-Hyperdoped Silicon Nanowires/Carbon Nanotube Bilayer Fabric as a High-Performance Lithium-Ion Battery Anode

Che-Bin Chang,[†] Chun-Yu Tsai,[†] Kuan-Ting Chen, and Hsing-Yu Tuan*

Cite This: https://doi.org/10.1021/acsaem.0c02932 Read Online

ACCESS | Metrics & More | Article Recommendations | Supporting Information

ABSTRACT: The solution synthetic method can produce large quantities of silicon nanowires (SiNWs) for various applications, such as energy storage, texturing and composites materials, etc. However, solution-grown SiNWs exhibit very low conductivity compared to chemical vapor deposition (CVD)-grown SiNWs due to their poor crystallinity or reaction byproducts such as insulating polysiliane or polyphenylsilane. Here, we report the large-scale synthesis of phosphorus-hyperdoped Si nanowires (PH-SiNWs) with atomic ratios of the P content ranging from 1 to 2 atom % via the tin(Sn)-seeded supercritical fluid−liquid−solid (SFLS) through the use of red P nanoparticles as dopant precursors. The resistivity of PH-SiNWs is 4.3×10^{-3} Ω·m, which is about 6 orders of magnitude lower than bulk silicon (Si) (1.86×10^{3} Ω·m) and about 3 orders of magnitude lower than intrinsic SiNWs (1.19 Ω·m). PH-SiNWs can be assembled on fabrics used as active materials for lithium-ion batteries, and combined with carbon nanotube fabric as current collectors, the bilayer fabrics can be used as freestanding independent lithium-ion battery anodes without the need for binders and additive. The PH-SiNWs/carbon nanotube (CNT) bilayer fabric anode reaches 820 mAh g^{-1} after 1000 cycles at a charge/discharge rate of 2 A g^{-1}, whereas the intrinsic SiNWs/CNT bilayer fabric only sustains its performance at the first 20 cycles. The PH-SiNWs/CNT bilayer fabric anode shows the first example of a solution-grown Si nanowire anode with a 1000-cycle life. The *ex situ* transmission electron microscopy (TEM) image shows that an evolved PH-SiNWs nanopore structure was formed after the cycle, whereas the intrinsic SiNWs anodes did not develop holes. This result can be attributed to the uniform doping of P in the Si nanowire, which enables the formation of nanopores for rapid lithium-ion transport tunnels.

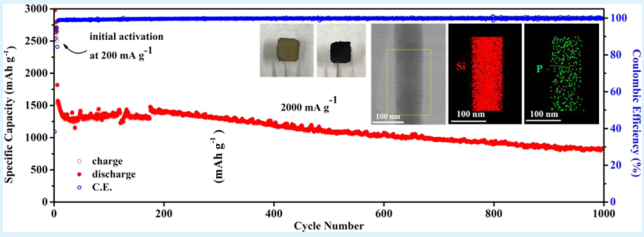

KEYWORDS: *silicon, nanowires, battery, lithium, energy storage*

INTRODUCTION

Hybrid electric vehicles (HEVs), electric vehicles (EVs), portable electronics, and plug-in hybrid electric vehicles (PHEVs) stimulate the demand for energy storage in pursuit of the high energy density and high cycle stability of lithium-ion batteries (LIBs).[1−3] However, the commercial anode material graphite only has a theoretical specific capacity of 372 mAh g^{-1}, which cannot meet the requirement of high energy density. Si is considered to be the most attractive alternative materials for graphite anodes, mainly because of its extremely high theoretical specific capacity (4200 mAh g^{-1}), similar working potential (0.5 V), and the second abundance in the earth crust.[4−6] When fully lithiated, the large volume expansion of Si (~400%, $Li_{15}Si_4$) causes the electrode to pulverize under these stresses and fall off the current collector.[7] In addition, the Si surface is unstable, and the formation of a solid electrolyte interphase (SEI) layer causes irreversible capacitance and eventually leads to a rapid decline in electrochemical performance.[8,9] Moreover, due to the inherent characteristics of Si as semiconductors and its relatively large internal ohmic resistance, its low electrochemical reaction rate limits the application of high-power LIBs (such as electric vehicles).[10]

To alleviate the mentioned problems, various Si nanostructures have been extensively studied in the past 10 years, such nanowires,[11−14] nanoparticles (NPs),[3,15] nanotubes,[16,17] thin films,[18,19] core−shell structure,[20] hollow Si sphere and porous Si to buffer volume changes, thereby improving the electrode stability.[21] The conductive buffer materials, such as carbon and copper, are usually used to cover the surface of Si to enhance the conductivity and mechanical strength.[13,22] However, the conductivity of internal Si is still low, and the coating may be still peeled off due to drastic changes in volume. Recently, the first-principle study showed that dopants such as phosphorus

Received: November 23, 2020
Accepted: March 21, 2021

(P) or boron (B) can affect the Li insertion energy into Si, which allows us to insert Li^+ into Si more easily.[23−25] Ohara et al. report that compared with intrinsic Si, the n-type Si can improve the power density and cycle life of the electrode.[26] Kang et al. reported that the doped Si nanowires have better specific capacity under high charge/discharge rates compared to nondoped ones.[27] P is the most widely used n-type dopant for Si wafers since it provides additional valence electrons and has a high diffusivity rate in Si.[28,29] Recent studies have shown that P dopant in SiNWs can help guide the formation of nanopore structures, which can withstand huge volume changes and increase the reaction area, thereby improving the overall battery performance.[30]

Compared with Si nanoparticles, SiNW is a representative nanostructure that can reduce the effect of massive volume change and mitigate materials cracking during electrochemical lithiation and delithiation. The chemical methods of SiNW synthesis can be divided into the gas phase and the solution phase methods. Compared to the gas method, the solution growth methods can provide a high yield and a large amount of SiNWs. Although vapor−liquid−solid (VLS) growth can effectively control the diameters of nanowires,[31] low yield is still the bottleneck of the VLS method, which may hinder its large-scale application.[12] Compared with the VLS method, the supercritical fluid−liquid−solid (SFLS) method can synthesize SiNWs in large quantities in few minutes.[32,33] The conductivity of P-doped and B-doped SiNWs is better than that of intrinsic SiNWs.[34] However, doping SiNWs with B, P atom is still challenging in solution synthesis, because it is hard to control B, P atom in the solution phase while the SiNWs grown, but through the red P nanoparticles (RPNPs) as P precursor and phenylsilane as Si precursor by SFLS method can be well doped and environment-friendly unlike the most widely used precursor P doping in chemical vapor deposition (CVD) is the addition of toxic PH_3 to the SiH_4 and the overall procedure required a strict factory environment.[35]

Here, we report the use of red P nanoparticles (RPNPs) as a P precursor and Sn as the seed to synthesize PH-SiNWs by the SFLS method. RPNPs is a stable particle that can be stored in an air environment without burning because red P is the most stable of three different types of P allotropes (red, white, and black),[36] as shown in Scheme 1. Briefly, a supercritical fluid−liquid−solid (SFLS) solution with RPNP powder, MPS, and $Sn(HMDS)_2$ as precursors was heated to 490 °C at a pressure at 800 psi and quenched by a water bath to obtain the product. The resistivity of PH-SiNWs is 4.3×10^{-3} Ω·m, which is about 6 orders of magnitude lower than that of bulk Si (1.86×10^3 Ω·m). In addition, we manufacture the bilayer fabric electrode, which is composed of PH-SiNWs and carbon nanotubes (CNTs), to increase the contact of electrolyte and current collectors without the use of conductive additives and binders.[37] As a result, the P-doped SiNWs/CNT bilayer fabric can maintain capacity retention of 55% after 1000 cycles, which shows that the solution-grown SiNWs have a high cycle stability potential for applications on LIBs. Moreover, the PH-SiNWs and intrinsic SiNWs after cycling were subjected to *ex situ* transmission electron microscopy (TEM) to study the structural difference after the Li reaction.

EXPERIMENTAL SECTION

Synthesis of RPNPs. RPNPs were synthesized based on the previous report.[28] First, 180 mg of cetyltrimethylammonium bromide (CTAB) was added into 30 mL of ethylene glycol. Then, 300 mg of RP and 3 g of iodine were put into a 20 mL sample vial in the glovebox. The vial was heated at 130 °C for 3 min and then put into a refrigerator to cool. After cooling, a purple-black solid was obtained and 10 mL of iodobenzene was injected into the vial, with ultrasonication until the solid completed dissolved. The iodobenzene solution was centrifuged to remove excess P and iodine and the liquid part was retained. Upon adding the liquid part into the CTAB solution, its color changed from colorless to orange. Finally, RPNPs were purified by 8000 rpm centrifugation using toluene and ethanol (1:2 vol %) three times to remove the residual ethylene glycol and byproducts. The RPNPs were then put in an argon-filled glovebox to avoid oxidation.

Scheme 1. Schematic Illustration of PH-SiNWs Synthesis by the SFLS Method

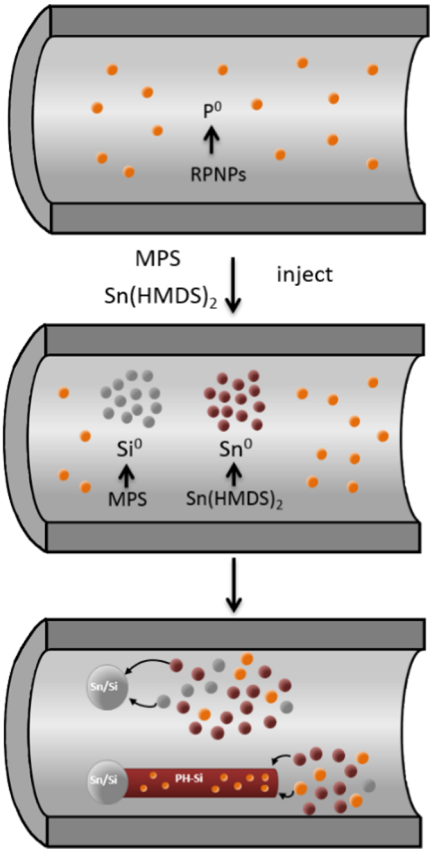

Synthesis and Characterization of PH-SiNWs. The SFLS method is used to synthesize Sn-seeded PH-SiNWs. First, to ensure that the Ti reactor is filled with argon, a reactor was placed in an argon-filled glovebox and then 4 mg of RPNPs powder was added to the reactor as a P source. Then, the reactor was sealed and taken out of the glovebox, and it was preheated to 490 °C by a heating block. Next, a PH-SiNW precursor containing 250 μL of phenylsilane (MPS), 36 μL of $Sn(HMDS)_2$, and 5 mL of anhydrous toluene (the ratio of Si and Sn is 22:1) was prepared. When the temperature reached 490 °C, and it was pressurized the reactor to 800 psi by a high-performance liquid chromatography (HPLC) pump (Lab Alloance, series 1500). The prepared precursor was injected into the six-way valve equipped with a 5 mL injection loop, which was connected to an HPLC pump. The reaction was injected into the reactor at a flow rate of 0.5 mL min^{-1}. After 15 min, the reactor was moved and cooled by a water bath for 30 min. The product was centrifuged at 8000 rpm for 5 min with a solution of toluene, ethanol, and chloroform in the ratio of 1:1:1 (v/v/v) to remove the byproducts. The morphologies of the P-doped SiNWs were characterized through field-emission scanning electron microscopy (FESEM, HITACHI SU8010) with a working distance of 8mm at 10 kV acceleration voltage and transmission electron microscopy (TEM,

https://doi.org/10.1021/acsaem.0c02932
ACS Appl. Energy Mater. XXXX, XXX, XXX−XXX

JEOL JEM-ARM200FTH) operated at 200 kV. X-ray diffraction (XRD) data was obtained from Rigaku Ultima IV. The surface P content was determined by a secondary ion mass spectrometer (SIMS).

Surface Passivation of PH-SiNWs. The PH-SiNWs were etched by 10% HCl for 15 min to remove the Sn seeds, and 10% hydrofluoric acid (HF) for 15 min to remove the oxidized part. After etching, the nanowires were rinsed with methanol to remove the residue HCl and HF. Fifteen milliliters of 1-dodecanethiol and etched PH-SiNWs were added to the sample vial and magnetically stirred at 80 °C for 12 h under an argon atmosphere. When the thiolation is complete, the product was centrifuged by a mixture of methanol and toluene in a volume ratio of 1:1 to remove excess 1-dodecanethiol. Finally, the product was placed in an argon-filled glovebox for further use.

Fabrication and Electrochemical Characterization of PH-SiNWs Fabric and PH-SiNWs/CNT. The PH-SiNW fabrics were fabricated by drop-casting the PH-SiNW toluene dispersion solution into the Teflon mold and left until the toluene completely evaporated. After drying, the SiNW fabric was peeled from the Teflon mold with a stamp tweezer. The PH-SiNWs/CNT fabrics were fabricated by two dispersion solutions; one was to disperse CNT in ethanol and the other was to disperse PH-SiNWs in toluene. First, the CNT dispersion was drop-cast into a Teflon mold and allowed to dry. After the ethanol has evaporated, PH-SiNWs were drop-cast into a Teflon mold. When the toluene was completely evaporated, the PH-SiNWs/CNT fabric was peeled from the mold using a stamp tweezer. The bilayer PH-SiNWs/CNT fabric was annealed at 800 °C in a tube furnace under an argon/hydrogen atmosphere. Finally, the fabrics were brought into the glovebox used to assemble the LIBs. The mass loading of the bilayer fabric is roughly 1.2−1.5 mg cm^{-2}.

The coin-type half-cell (CR2032) was assembled in an argon-filled glovebox using Li metal foil as a counter electrode. The electrolyte composed of 1 M $LiPF_6$ in ethylene carbonate/diethyl carbonate/fluoroethylene carbonate (EC/DEC/FEC) (5:5:1 at v/v/v) was added to infiltrate the bilayer fabric and PP/PE/PP separator was added, followed by the Li foil. After crimping, the battery was taken out from the glovebox and the electrochemical performance was tested by a Maccor Series 4000 battery test system with the voltage ranging from 0.01 to 1.50 V.

RESULTS AND DISCUSSION

The X-ray diffraction (XRD) pattern (Figure 1) shows that the synthesized Sn-seeded PH-SiNWs have good crystallinity,

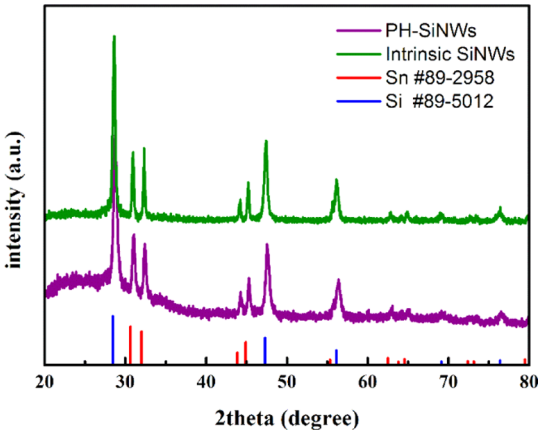

Figure 1. XRD pattern of PH-SiNWs and intrinsic SiNWs.

which contains a large amount of crystalline Si. SiNW has been confirmed to exist in face-centered cubic Si (JCPDS No. 89-5012) and Sn seed exists in tetragonal Sn (JCPDS No. 89-2958). According to metal-seeded growth, Sn exists in the tip particles of nanowires.[37] To eliminate the effect of Sn on battery performance, Sn particles were removed by soaking in 10% HCl solution for 15 min and XRD was further utilized to characterize PH-SiNWs. In the XRD pattern (Figure S1a, Supporting Information), the original Sn peaks were disappeared due to HCl. The SEM image (Figure S1b, Supporting Information) shows that the Sn seed at the tip of PH-SiNWs was removed. Figure 2 is an SEM image of PH-SiNW with Sn as a seed. The atomic ratio of Si and Sn appears to result in the kinking of the nanowires. When the atomic ratio of Si increases (32:1), the nanowires are seriously kinked, and the surface is covered by a thick layer of polyphenylsilane shell.[38] Therefore, the suitable atomic ratio of Si and Sn for the precursor solution is 22:1 to form an appropriate polyphenylsilane shell. In Figure 2b, most products have a length of tens of microns, an average diameter of about 60 ± 10 nm, and the surface is not covered with a thick polyphenylsilane shell. The SFLS-grown SiNWs appear to combine (Figure 2a,b), which is suitable for fabric electrode manufacturing (Figure S2, Supporting Information). The Sn particles observed at the tip of the nanowire (Figure 2c) confirmed the growth mechanism of SFLS.[39] Through energy-dispersive spectroscopy (EDS) mapping analysis (Figure S3, Supporting Information), no Sn signal was detected. After the Sn seed was etched, the surface was modified with dodcanethiol to disperse the stable solvent, which is beneficial to the preparation of PH-SiNWs/CNT fabrics.[39] The nanowire solution was dropped on a Teflon mold to make a fabric composed of dense PH-SiNWs.

The TEM image of a single PH-SiNW is shown in Figure 3a. The P distribution in PH-SiNWs was confirmed by energy-dispersive spectroscopy (EDS) (Figure 3b,c). A high concentration of P is uniformly doped in SiNWs. Koren et al. reported that, through the VLS method, the P concentration distribution in PH-SiNWs varies with the radius. The difference between the core layer and the outermost is 2 orders of magnitude, which affects the electrochemical performance.[40] Line scans were performed along the growth axis (Figure 3d) and through PH-SiNWs (Figure 3e). The P concentration was 2 atom % in units of 10 nm along the growth direction of the nanowire, and secondary ion mass spectrometry was also conducted (Figure S4, Supporting Information) to further confirm the P concentration variation with depth in PH-SiNWs. The above evidence shows that there is no significant difference in the distribution of P throughout the whole body of a nanowire. Compared with thick SiNWs, PH-SiNWs with a diameter of less than 200 nm has extremely strong mechanical stability. Through the TEM observation, the diameter of PH-SiNWs was found lower than the critical diameter, which made PH-SiNWs have strong mechanical stability.[41]

To understand the effect of P doping on the conductivity of SiNWs, we used two-terminal $I-V$ measurements. The PH-SiNW was supported on a silicon dioxide substrate, and the back gate conducts Si. The electrical conductivity is measured by a computer-controlled system with ≤1 pA noise. The PH-SiNWs and intrinsic SiNWs devices integrated in the IV measurements of the two-point measurement modules are shown in Figure 4a. The resistivity of PH-SiNWs is 4.3×10^{-3} Ω·m, which was about 6 orders of magnitude lower than that of bulk Si (1.86×10^{3} Ω·m) and about 3 orders of magnitude lower than that of intrinsic Si (1.19 Ω·m). This proves that P doping can significantly improve the conductivity of SiNWs. The field effect can be observed in the general characterization of SiNWs,[42] so we used different gate-to-source voltage to

https://doi.org/10.1021/acsaem.0c02932
ACS Appl. Energy Mater. XXXX, XXX, XXX−XXX

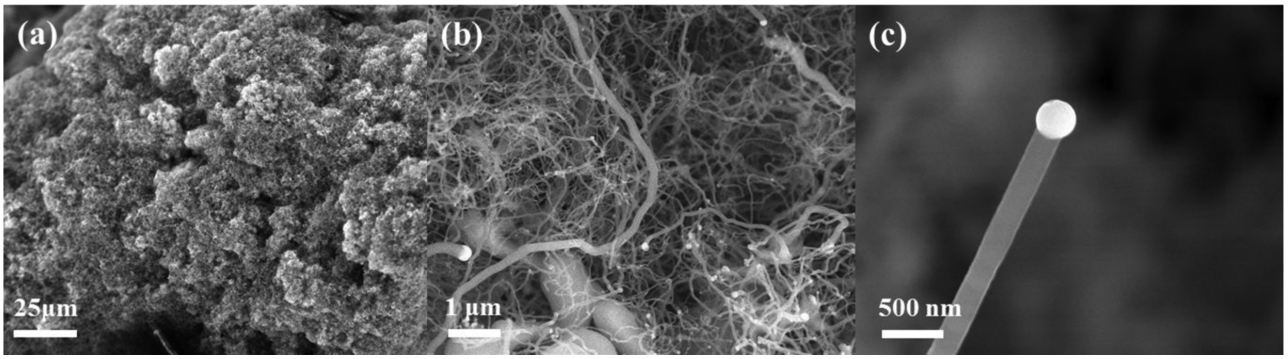

Figure 2. Morphology of PH-SiNWs. (a) Low-magnification SEM image of PH-SiNWs, (b) high-magnification SEM image of PH-SiNWs, and (c) high-magnification SEM image of the seeded on the PH-SiNWs.

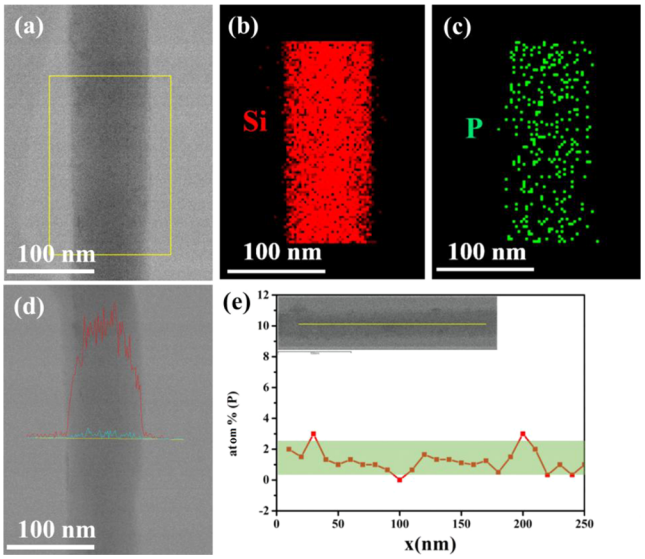

Figure 3. (a), (b), (c) EDS element mapping of PH-SiNWs. Red and green represent P and Si, respectively. (d) EDS line scan across PH-SiNWs. (e) EDS line scans along the nanowire growth axis.

identify the characteristics of PH-SiNWs (Figure 4b) and no field-effect response was found on the back-gated nanowire field-effect transistor.

Figure 5 reveals that the amount of RPNPs added has an effect on the morphology of PH-SiNWs. According to the previous report on the growth mechanism of SiNWs synthesized by the SFLS methods, Sn and Si form a eutectic and are decomposed by monopenylsilane to produce SiH_4, and SiH_4 decomposes into atomic Si. RPNPs sublimated into P atomic state in a high-pressure environment and participate in the growth of SiNWs.[43] The amount of P added has a significant effect on the form of the product. When 20 mg of RPNP is added to the reaction solution, the final product contains many P particles and only a few nanowires are formed (Figure 5a). Too many P particles affect the overall conductivity performance. Although the addition of RPNPs was reduced to 15 mg, it shows that some short and wide nanowires were formed and mixed with many P particles (Figure 5b). The addition of excess RPNPs hindered the formation of nanowires, so RPNPs were further reduced to 10 mg (Figure 5c). An increase in nanowire production was observed, but many P particles were formed at the same time. To reduce P particles, the optimal amount of RPNPs added into the reaction is 4 mg (Figure 5d). The nanowire fabric was annealed at 800 °C to remove excess P particles to convert polyphenylsilane shell to a conductive carbon skin.[38] In fact, annealing treatment makes the distribution of P more uniform and enhances the conductivity.[44] As shown in Figure S5, Supporting Information, there are almost no P particles after annealing.

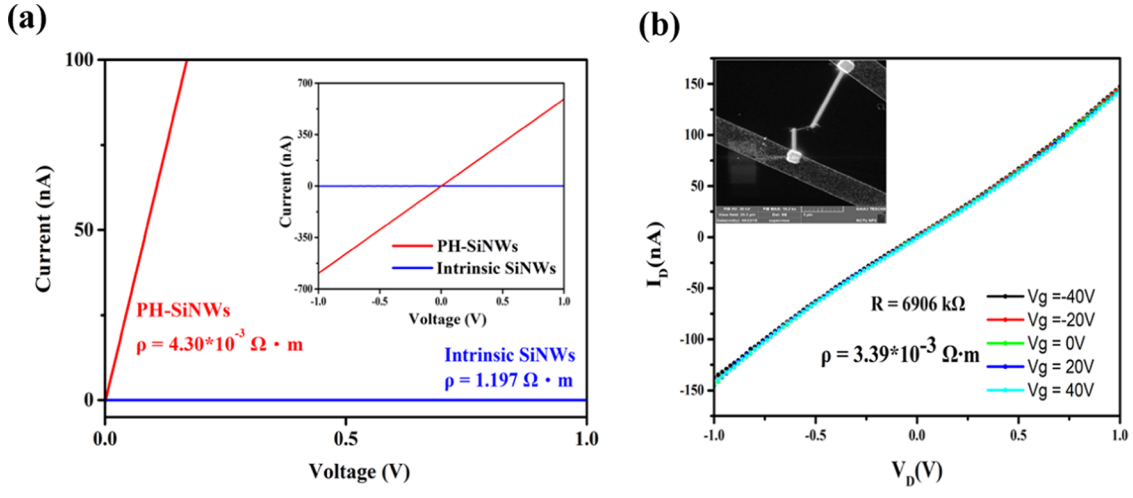

Figure 4. (a) Two-probe $I-V$ measurements of PH-SiNWs and intrinsic SiNWs for comparison. (b) $I-V$ curve of PH-SiNWs with different V_g.

https://doi.org/10.1021/acsaem.0c02932
ACS Appl. Energy Mater. XXXX, XXX, XXX−XXX

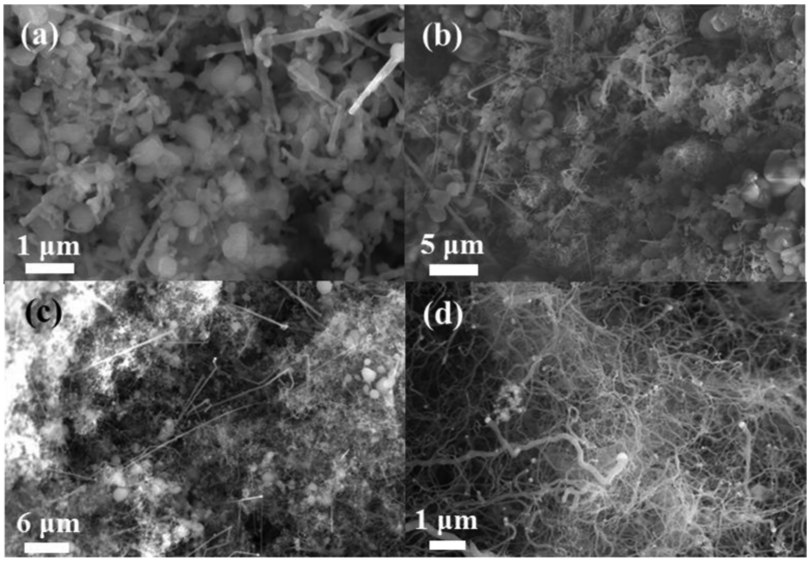

Figure 5. PH-SiNW synthesis by different amounts of RPNPs. (a) PH-SiNWs synthesized by 20 mg of RPNPs. (b) PH-SiNWs synthesized by 15 mg of RPNPs. (c) PH-SiNWs synthesized by 10 mg of RPNPs. (d) PH-SiNWs synthesized by 4 mg of RPNPs.

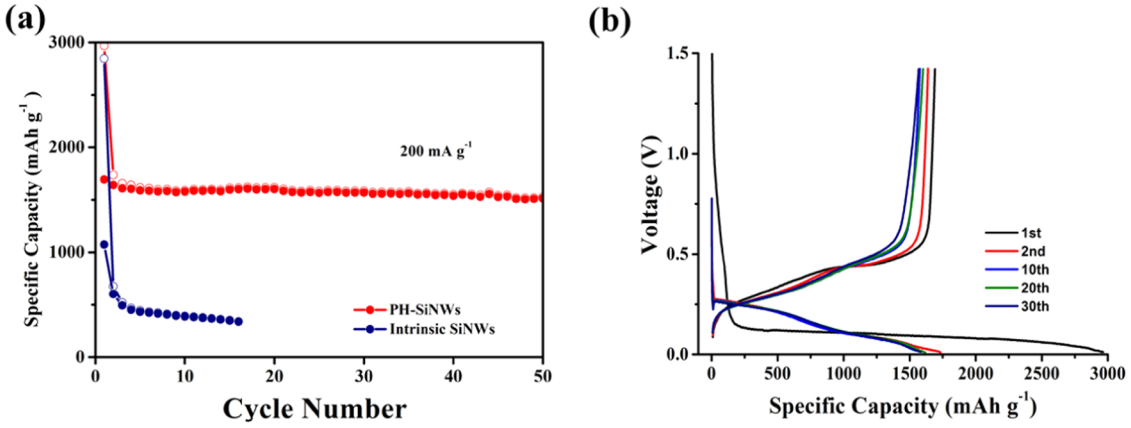

Figure 6. (a) Cycling performance of PH-SiNWs and intrinsic SiNWs in 50 cycles at 200 mA g^{-1} current density. (b) Charge/discharge profile of PH-SiNWs at 200 mA g^{-1} current density.

SiNWs can be used as anodes in combination with other carbon nanomaterials. These carbon nanomaterials can be used the support for freestanding and binder-free lithium-ion battery anodes. The bilayer fabric structure provides increased contact with the electrolyte and current collector to expand the reaction area. The electrochemical performance of PH-SiNWs/CNT and intrinsic SiNWs/CNT in Figure 7a−c is achieved using coin-typed cells (CR2032) by galvanostatic charge/discharge technology at a current density of 2000 mA g^{-1} in the voltage ranging from 0.01 to 1.50 V. The mass load of active materials (PH-SiNWs and intrinsic SiNWs) is about 1.0−1.5 mg cm^{-2}. It can be seen from Figure 6b that during the first discharge, the voltage curve is long and flat. According to the previous reports, crystalline Si and Li form amorphous Li_xSi, and the subsequent discharge and charge cycle curves show different amorphous Si. In addition, no Sn plateau was observed.[45] It is worth noting that in Figure 6a, the first discharge capacity of PH-SiNWs and intrinsic SiNWs are 2967 and 2845 mA g^{-1}, respectively, and the corresponding Coulombic efficiencies are 57 and 37%, respectively. In the first cycle, the Coulombic efficiency of PH-SiNWs increased by 20% compared with that of the intrinsic Si nanowires, and its performance may be attributed to its excellent conductivity.[23,46] In the subsequent charge and discharge cycles, the capacity hardly decayed, and the 50th cycle still showed a capacity of 1500 mAh g^{-1}, which confirmed the advantages of PH-SiNWs. The charge/discharge curve and cycling performance of CNT fabric are available in Figure S6, Supporting Information; at the high current density of 2 A g^{-1}, the CNT fabric only contributed a specific capacity of 100 mAh g^{-1}. On the basis of this condition, the CNT fabric specific capacity contribution is ignorable.

Figure 7a is a graph of the charge/discharge curves of PH-SiNWs at different current densities. The specific capacities of PH-SiNWs are 1280, 1050, 850, 690, 580, 460, and 230 mAh g^{-1} at the current densities of 200, 400, 1000, 2000, 4000, 6000, and 10 000 mA g^{-1}, respectively. This shows that even at a current density of 6000 mA g^{-1}, its specific capacity is still higher than that of graphite (372 mA g^{-1}). In addition, when the current density of 200 mA g^{-1} was restored, the recovery capacity was 1280 mA g^{-1}, indicating that PH-SiNWs have good mechanical structural stability. Figure 7b shows the voltage curves of electrodes cycled at different charge/discharge rates, which exhibit a typical Si anode lithiation/

https://doi.org/10.1021/acsaem.0c02932
ACS Appl. Energy Mater. XXXX, XXX, XXX−XXX

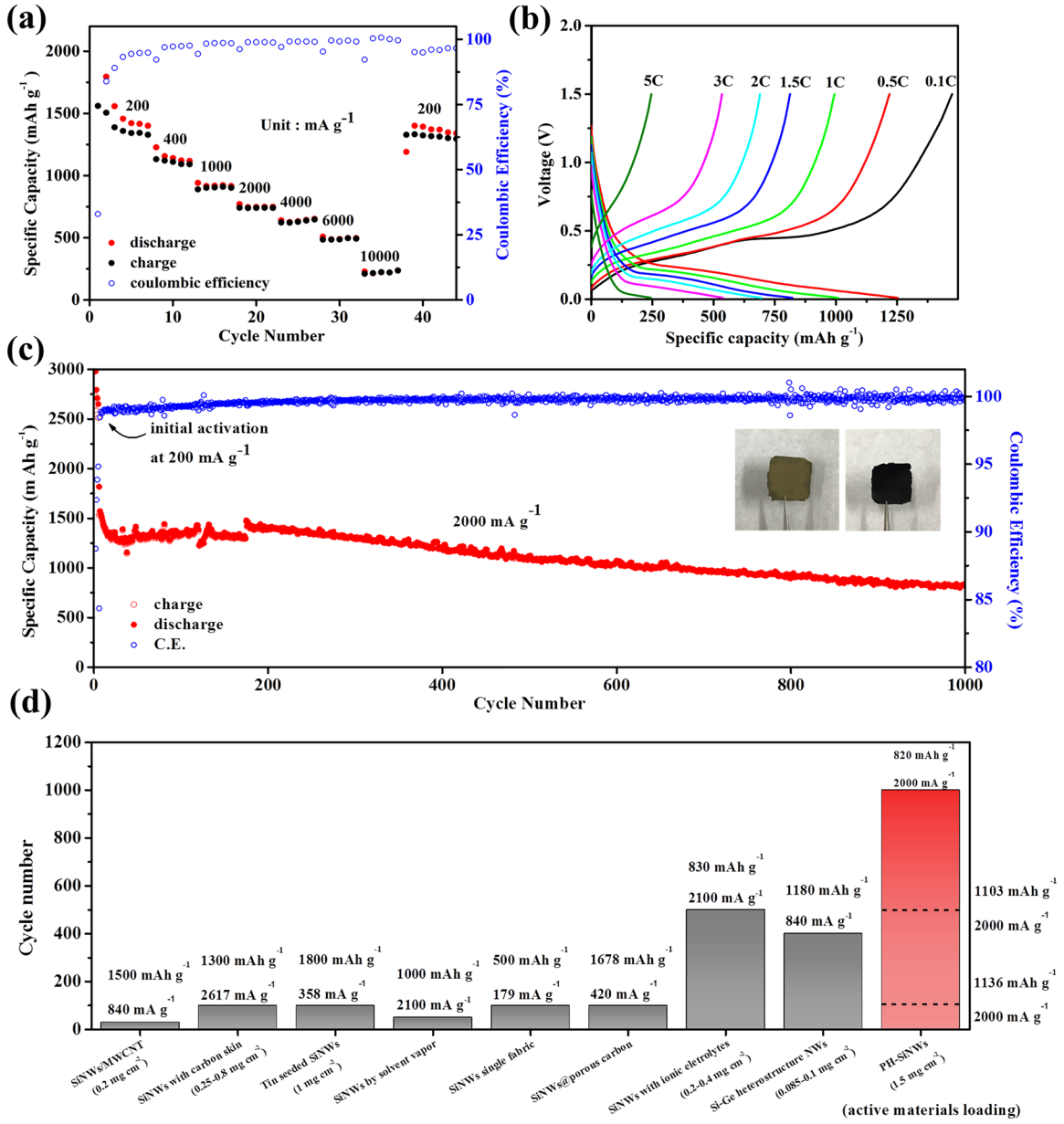

Figure 7. (a) Rate performance of PH-SiNWs at various current densities from 200 to 10 000 mA g^{-1}. (b) Charge/discharge profiles of PH-SiNWs at various current densities from 200 to 10 000 mA g^{-1}. (c) Cycling stability of PH-SiNWs at a high current density of 2000 mA g^{-1}. Inset: front and back images of the PH-SiNWs/CNT bilayer fabric. (d) Comparison of cycle stability between PH-SiNWs and the as-reported solution-grown SiNWs.

delithiation voltage curve at different charge/discharge rates. Figure 7c shows the stability of the long cycle performed at a current density of 200 mAh g^{-1} in the first three cycles. In the subsequent charge/discharge cycle at 2000 mAh g^{-1}, the specific capacity of the bilayer fabric was maintained at 820 mAh g^{-1}, which had a capacity retention rate of 55% compared to the 10th cycle. The higher mass loading of active materials in PH-SiNWs/CNT (3.7 mg cm^{-2}) bilayer fabric electrode cycling performance was provided (Figure S7, Supporting Information). The higher active materials loading reduces the mechanical strength, which hard to manufacture fabric electrode, even decrease the conductivity between SiNWs and CNT current collector, causing poor cycle stability and specific capacity. The PH-SiNWs/CNT bilayer fabric has excellent electrochemical performance because P doping greatly improves the electric conductivity of the internal Si structure, and the electrode design of the bilayer fabric allows better contact between the active material and the current collector. The cycle stability of PH-SiNWs and the reported solution-grown SiNWs are compared in Figure 7d.[12,33,38,47−52] At a rate of 2000 mA g^{-1}, PH-SiNW shows excellent specific capacity and cycle stability. Zhu et al. studied the *in situ* TEM of P-doped SiNWs, when P-doped SiNWs during the delithiation process, the delithiation rate was higher than undoped SiNWs, leading to Si atoms can't rearrangement, and form the nanopores structure. It is worth mentioning that nanopores will be annihilated by Li reinsertion reported by Zhu et al.; however, in our work, PH-SiNWs still maintain the nanoporous structure after 1000 cycles.[30] We believe that the uniformity of P doping affects the occurrence of pores, and the solution-phase SFLS synthesis method has an advantage of the uniformity of P doping, which further affects the formation of

https://doi.org/10.1021/acsaem.0c02932
ACS Appl. Energy Mater. XXXX, XXX, XXX−XXX

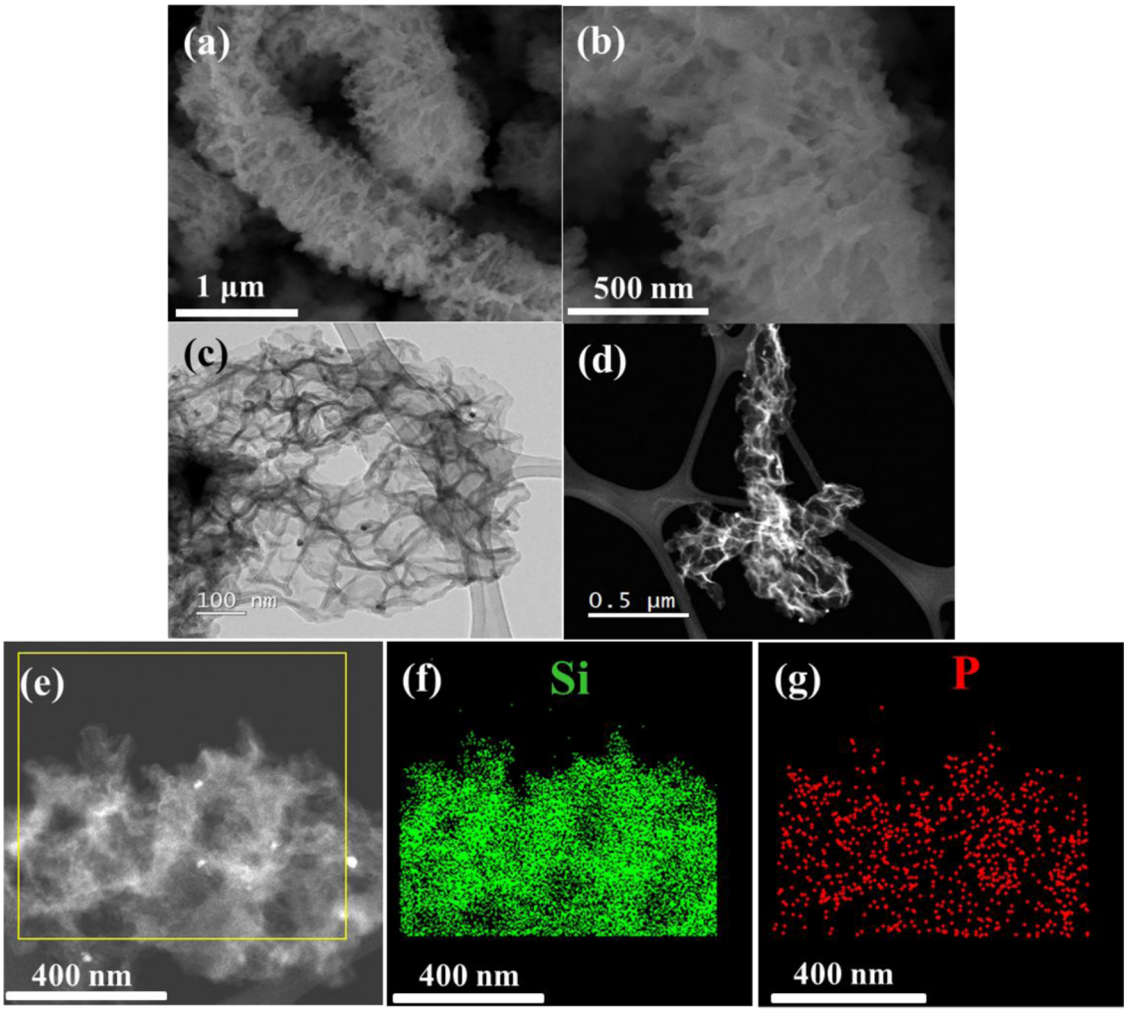

Figure 8. (a), (b) SEM images of PH-SiNWs after 1000 cycles. (c) Bright-field TEM image of P-doped SiNWs after 1000 cycles. (d) Dark-field TEM image of PH-SiNWs after 1000 cycles. (e)−(g) TEM image and element mapping images of Si, P after 1000 cycles.

the pore structures. After 1000 cycles (Figure 8a), the width of PH-SiNWs was expanded, and the nanowire structure developed many vacancies, which confirms that the pore structure caused by P doping can buffer severe volume change. In addition, a large number of pores can be observed on PH-SiNWs, whereas no pore structure formation is observed on intrinsic SiNWs (Figure S8, Supporting Information). In the bright-field TEM picture (Figure 8c), it can be clearly observed that due to the vacancies, the cycled PH-SiNWs form a porous network structure, which is more obvious in the dark-field TEM image (Figure 8d). This porous network structure can provide a fast lithium-ion transport tunnel to expand the reaction area.[47,53−56] Therefore, in addition to the bilayer fabric structure with better contact with the current collector, the formation of nanopores during the charge/discharge test is why such a long cycle life and high specific capacity can be achieved without binders and conductive agents. On the other hand, the TEM mapping (Figure 8e−g) shows that the phosphorus is distributed evenly in the pore structure after 1000 cycles of the lithiation/delithiation process, which proves that the SFLS method allows the phosphorus to be uniformly doped in SiNWs.

CONCLUSIONS

In summary, we report the one-step synthesis of PH-SiNWs via the SFLS method, which can provide a large amount of output with simple steps. Moreover, PH-SiNW has a significantly improved conductivity. The resistivity of PH-SiNWs is 4.3×10^{-3} Ω·m, which is about 6 orders of magnitude lower than that of bulk Si (1.86×10^{3} Ω·m). PH-SiNWs exhibit impressive current density and durability. At a high current density of 6000 mA g^{-1}, the PH-SiNWs still have a specific capacity of 460 mA g^{-1}, and the reversible capacity is 820 mAh g^{-1} after 1000 cycles. The excellent performance at high current density is mainly because the SiNWs are uniformly doped with P. In addition, the presence of nanopores in the SiNWs was observed in the SEM and TEM images after 1000 cycles. These nanopores are considered to be the main reason for the good long-cycle stability. The small diameters (60 ± 10 nm) of SiNWs obtained from the SFLS method are smaller than the critical pulverized diameter (220−260 nm), which can prevent serious cracks during the lithiation/delithiation process. On the other hand, using CNT as a current collector, a combination of weight reduction and total energy density can be achieved. Therefore, the PH-SiNWs/CNT bilayer fabric structure has high cycle stability and rapid charge and

https://doi.org/10.1021/acsaem.0c02932
ACS Appl. Energy Mater. XXXX, XXX, XXX−XXX

discharge capability, and it is considered to meet the future development needs of lithium-ion batteries.

■ ASSOCIATED CONTENT

Supporting Information

The Supporting Information is available free of charge at https://pubs.acs.org/doi/10.1021/acsaem.0c02932.

Material; photograph and SEM and TEM images of PH-SiNWs and intrinsic SiNWs; EDS analysis of PH-SiNWs; secondary ion mass spectrometry (SIMS) of PH-SiNWs; additional $I-V$ curve of PH-SiNWs with different V_g; and rate performance of intrinsic SiNWs at various current densities (PDF)

■ AUTHOR INFORMATION

Corresponding Author

Hsing-Yu Tuan − *Department of Chemical Engineering, National Tsing Hua University, Hsinchu 30013, Taiwan;* orcid.org/0000-0003-2819-2270; Phone: (886)3-571-5131; Email: hytuan@che.nthu.edu.tw

Authors

Che-Bin Chang − *Department of Chemical Engineering, National Tsing Hua University, Hsinchu 30013, Taiwan*

Chun-Yu Tsai − *Department of Chemical Engineering, National Tsing Hua University, Hsinchu 30013, Taiwan*

Kuan-Ting Chen − *Department of Chemical Engineering, National Tsing Hua University, Hsinchu 30013, Taiwan*

Complete contact information is available at: https://pubs.acs.org/10.1021/acsaem.0c02932

Author Contributions

†C.-B.C. and C.-Y.T. contributed equally to this work.

Notes

The authors declare no competing financial interest.

■ ACKNOWLEDGMENTS

This work was financially supported by the Young Scholar Fellowship Program by the Ministry of Science and Technology in Taiwan, under grants of MOST 108-2636-E-007-013, MOST 108-2622-8-007-016, and MOST 109-2636-E-007-011. The authors also acknowledge the financial support of the National Tsing Hua University through the grant of 107Q2708E1.

■ REFERENCES

(1) Armand, M.; Tarascon, J.-M. Building better batteries. *Nature* **2008**, *451*, 652−657.

(2) Scrosati, B. Challenge of portable power. *Nature* **1995**, *373*, 557−558.

(3) Wu, H.; Yu, G.; Pan, L.; Liu, N.; McDowell, M. T.; Bao, Z.; Cui, Y. Stable Li-ion battery anodes by *in situ* polymerization of conducting hydrogel to conformally coat silicon nanoparticles. *Nat. Commun* **2013**, *4*, No. 1943.

(4) Kamali, A. R.; Fray, D. J. Tin-based materials as advanced anode materials for lithium ion batteries: a review. *Rev. Adv. Mater. Sci* **2011**, *27*, 14−24.

(5) Chan, C. K.; Ruffo, R.; Hong, S. S.; Huggins, R. A.; Cui, Y. Structural and electrochemical study of the reaction of lithium with silicon nanowires. *J. Power Sources* **2009**, *189*, 34−39.

(6) Zhang, F.; Wan, L.; Chen, J.; Li, X.; Yan, X. Crossed carbon skeleton enhances the electrochemical performance of porous silicon nanowires for lithium ion battery anode. *Electrochim. Acta* **2018**, *280*, 86−93.

(7) Xu, Y. H.; Yin, G. P.; Zuo, P. J. Geometric and electronic studies of $Li_{15}Si_4$ for silicon anode. *Electrochim. Acta* **2008**, *54*, 341−345.

(8) Boukamp, B.; Lesh, G.; Huggins, R. All-solid lithium electrodes with mixed-conductor matrix. *J. Electrochem. Soc* **1981**, *128*, No. 725.

(9) Chan, C. K.; Ruffo, R.; Hong, S. S.; Cui, Y. Surface chemistry and morphology of the solid electrolyte interphase on silicon nanowire lithium-ion battery anodes. *J. Power Sources* **2009**, *189*, 1132−1140.

(10) Rousselot, S.; Gauthier, M.; Mazouzi, D.; Lestriez, B.; Guyomard, D.; Roué, L. Synthesis of boron-doped Si particles by ball milling and application in Li-ion batteries. *J. Power Sources* **2012**, *202*, 262−268.

(11) Burchak, O.; Keller, C.; Lapertot, G.; Salaün, M.; Danet, J.; Chen, Y.; Bendiab, N.; Pépin-Donat, B.; Lombard, C.; Faure-Vincent, J. Scalable chemical synthesis of doped silicon nanowires for energy applications. *Nanoscale* **2019**, *11*, 22504−22514.

(12) Chan, C. K.; Patel, R. N.; O'connell, M. J.; Korgel, B. A.; Cui, Y. Solution-grown silicon nanowires for lithium-ion battery anodes. *ACS Nano* **2010**, *4*, 1443−1450.

(13) Chen, H.; Xiao, Y.; Wang, L.; Yang, Y. Silicon nanowires coated with copper layer as anode materials for lithium-ion batteries. *J. Power Sources* **2011**, *196*, 6657−6662.

(14) Wang, X.; Li, G.; Seo, M. H.; Lui, G.; Hassan, F. M.; Feng, K.; Xiao, X.; Chen, Z. interfaces Carbon-coated silicon nanowires on carbon fabric as self-supported electrodes for flexible lithium-ion batteries. *ACS Appl. Mater. Interfaces* **2017**, *9*, 9551−9558.

(15) Lee, J. K.; Smith, K. B.; Hayner, C. M.; Kung, H. H. Silicon nanoparticles−graphene paper composites for Li ion battery anodes. *Chem. Commun.* **2010**, *46*, 2025−2027.

(16) Park, M.-H.; Kim, M. G.; Joo, J.; Kim, K.; Kim, J.; Ahn, S.; Cui, Y.; Cho, J. Silicon nanotube battery anodes. *Nano Lett.* **2009**, *9*, 3844−3847.

(17) Song, T.; Xia, J.; Lee, J.-H.; Lee, D. H.; Kwon, M.-S.; Choi, J.-M.; Wu, J.; Doo, S. K.; Chang, H.; Park, W. I. Arrays of sealed silicon nanotubes as anodes for lithium ion batteries. *Nano Lett.* **2010**, *10*, 1710−1716.

(18) Maranchi, J.; Hepp, A.; Kumta, P. High capacity, reversible silicon thin-film anodes for lithium-ion batteries. *Electrochem. Solid-State Lett.* **2003**, *6*, No. A198.

(19) Takamura, T.; Ohara, S.; Uehara, M.; Suzuki, J.; Sekine, K. A vacuum deposited Si film having a Li extraction capacity over 2000 mAh/g with a long cycle life. *J. Power Sources* **2004**, *129*, 96−100.

(20) Xu, Y.; Yin, G.; Ma, Y.; Zuo, P.; Cheng, X. Nanosized core/shell silicon@ carbon anode material for lithium ion batteries with polyvinylidene fluoride as carbon source. *J. Mater. Chem.* **2010**, *20*, 3216−3220.

(21) Yao, Y.; McDowell, M. T.; Ryu, I.; Wu, H.; Liu, N.; Hu, L.; Nix, W. D.; Cui, Y. Interconnected silicon hollow nanospheres for lithium-ion battery anodes with long cycle life. *Nano Lett.* **2011**, *11*, 2949−2954.

(22) Kim, J. W.; Ryu, J. H.; Lee, K. T.; Oh, S. M. Improvement of silicon powder negative electrodes by copper electroless deposition for lithium secondary batteries. *J. Power Sources* **2005**, *147*, 227−233.

(23) Kim, J. S.; Choi, W.; Byun, D.; Lee, J. K. Electrochemical characteristics of phosphorus doped silicon for the anode material of lithium secondary batteries. *Solid State Ionics* **2012**, *212*, 43−46.

(24) Long, B. R.; Chan, M. K.; Greeley, J. P.; Gewirth, A. A. Dopant modulated Li insertion in Si for battery anodes: theory and experiment. *J. Phys. Chem. C* **2011**, *115*, 18916−18921.

(25) Ren, Y.; Zhou, X.; Tang, J.; Ding, J.; Chen, S.; Zhang, J.; Hu, T.; Yang, X.-S.; Wang, X.; Yang, J. Boron-Doped Spherical Hollow-Porous Silicon Local Lattice Expansion toward a High-Performance Lithium-Ion-Battery Anode. *Inorg. Chem.* **2019**, *58*, 4592−4599.

(26) Ohara, S.; Suzuki, J.; Sekine, K.; Takamura, T. A thin film silicon anode for Li-ion batteries having a very large specific capacity and long cycle life. *J. Power Sources* **2004**, *136*, 303−306.

(27) Kang, K.; Lee, H.-S.; Han, D.-W.; Kim, G.-S.; Lee, D.; Lee, G.; Kang, Y.-M.; Jo, M.-H. Maximum Li storage in Si nanowires for the high capacity three-dimensional Li-ion battery. *Appl. Phys. Lett.* **2010**, *96*, No. 053110.
(28) Chang, W.-C.; Tseng, K.-W.; Tuan, H.-Y. Solution synthesis of iodine-doped red phosphorus nanoparticles for lithium-ion battery anodes. *Nano Lett.* **2017**, *17*, 1240−1247.
(29) Fu, Y.; Wei, Q.; Zhang, G.; Sun, S. Advanced phosphorus-based materials for lithium/sodium-ion batteries: recent developments and future perspectives. *Adv. Energy Mater.* **2018**, *8*, No. 1703058.
(30) Zhu, J.; Guo, M.; Liu, Y.; Shi, X.; Fan, F.; Gu, M.; Yang, H. In Situ TEM of Phosphorus-Dopant-Induced Nanopore Formation in Delithiated Silicon Nanowires. *ACS Appl. Mater. Interfaces* **2019**, *11*, 17313−17320.
(31) Park, Y.-H.; Kim, J.; Kim, H.; Kim, I.; Lee, K.-Y.; Seo, D.; Choi, H.-J.; Kim, W. Thermal conductivity of VLS-grown rough Si nanowires with various surface roughnesses and diameters. *Appl. Phys. A* **2011**, *104*, 7−14.
(32) Holmes, J. D.; Johnston, K. P.; Doty, R. C.; Korgel, B. A. Control of thickness and orientation of solution-grown silicon nanowires. *Science* **2000**, *287*, 1471−1473.
(33) Chockla, A. M.; Klavetter, K. C.; Mullins, C. B.; Korgel, B. Tin-seeded silicon nanowires for high capacity Li-ion batteries. *Chem. Mater.* **2012**, *24*, 3738−3745.
(34) Alvarez, J.; Ngo, I.; Gueunier-Farret, M.-E.; Kleider, J.-P.; Yu, L.; Cabarrocas, P. R.; Perraud, S.; Rouvière, E.; Celle, C.; Mouchet, C. Conductive-probe atomic force microscopy characterization of silicon nanowire. *Nanoscale Res. Lett.* **2011**, *6*, No. 110.
(35) Tanaka, Y.; Furata, M.; Mastuura, H.; Nakano, N.; Fujishima, A.; Honda, K. Development of High-sensitive Gas-sensor for B_2H_6 using Gas-permeable Conductive DLC Membrane. *ECS Trans.* **2008**, *16*, No. 387.
(36) Chan, C.-Y.; Chang, C.-H.; Tuan, H.-Y. Colloidal synthesis of porous red phosphorus nanoparticles as a metal-free electrocatalyst for the hydrogen evolution reaction. *Chem. Commun.* **2020**, *56*, 2937−2940.
(37) Lai, C.-M.; Kao, T.-L.; Tuan, H.-Y. Si nanowires/Cu nanowires bilayer fabric as a lithium ion capacitor anode with excellent performance. *J. Power Sources* **2018**, *379*, 261−269.
(38) Bogart, T. D.; Oka, D.; Lu, X.; Gu, M.; Wang, C.; Korgel, B. A. Lithium ion battery performance of silicon nanowires with carbon skin. *ACS Nano* **2014**, *8*, 915−922.
(39) Yuan, F.-W.; Yang, H.-J.; Tuan, H.-Y. Alkanethiol-passivated Ge nanowires as high-performance anode materials for lithium-ion batteries: the role of chemical surface functionalization. *ACS Nano* **2012**, *6*, 9932−9942.
(40) Koren, E.; Berkovitch, N.; Rosenwaks, Y. Measurement of active dopant distribution and diffusion in individual silicon nanowires. *Nano Lett.* **2010**, *10*, 1163−1167.
(41) Ryu, I.; Choi, J. W.; Cui, Y.; Nix, W. D. Size-dependent fracture of Si nanowire battery anodes. *J. Mech. Phys. Solids* **2011**, *59*, 1717−1730.
(42) Koo, S.-M.; Edelstein, M. D.; Li, Q.; Richter, C. A.; Vogel, E. M. Silicon nanowires as enhancement-mode Schottky barrier field-effect transistors. *Nanotechnology* **2005**, *16*, No. 1482.
(43) Lu, X.; Hanrath, T.; Johnston, K. P.; Korgel, B. A. Growth of single crystal silicon nanowires in supercritical solution from tethered gold particles on a silicon substrate. *Nano Lett.* **2003**, *3*, 93−99.
(44) Oehrlein, G.; Cohen, S.; Sedgwick, T. Diffusion of phosphorus during rapid thermal annealing of ion-implanted silicon. *Appl. Phys. Lett.* **1984**, *45*, 417−419.
(45) Son, S. B.; Trevey, J. E.; Roh, H.; Kim, S. H.; Kim, K. B.; Cho, J. S.; Moon, J. T.; DeLuca, C. M.; Maute, K. K.; Dunn, M. L. Microstructure study of electrochemically driven Li_xSi. *Adv. Energy Mater.* **2011**, *1*, 1199−1204.
(46) Wang, C.; Appleby, A. J.; Little, F. E. Electrochemical study on nano-Sn, Li4. 4Sn and AlSi0. 1 powders used as secondary lithium battery anodes. *J. Power Sources* **2001**, *93*, 174−185.
(47) Ge, M.; Rong, J.; Fang, X.; Zhou, C. Porous doped silicon nanowires for lithium ion battery anode with long cycle life. *Nano Lett.* **2012**, *12*, 2318−2323.
(48) Chockla, A. M.; Harris, J. T.; Akhavan, V. A.; Bogart, T. D.; Holmberg, V. C.; Steinhagen, C.; Mullins, C. B.; Stevenson, K. J.; Korgel, B. A. Silicon nanowire fabric as a lithium ion battery electrode material. *J. Am. Chem. Soc.* **2011**, *133*, 20914−20921.
(49) Zhao, X.; Rui, X.; Zhou, W.; Tan, L.; Yan, Q.; Lu, Z.; Hng, H. H. Growth of Si nanowires in porous carbon with enhanced cycling stability for Li-ion storage. *J. Power Sources* **2014**, *250*, 160−165.
(50) Mullane, E.; Kennedy, T.; Geaney, H.; Dickinson, C.; Ryan, K. M. Synthesis of tin catalyzed silicon and germanium nanowires in a solvent−vapor system and optimization of the seed/nanowire interface for dual lithium cycling. *Chem. Mater.* **2013**, *25*, 1816−1822.
(51) Kim, G.-T.; Kennedy, T.; Brandon, M.; Geaney, H.; Ryan, K. M.; Passerini, S.; Appetecchi, G. B. Behavior of germanium and silicon nanowire anodes with ionic liquid electrolytes. *ACS Nano* **2017**, *11*, 5933−5943.
(52) Stokes, K.; Flynn, G.; Geaney, H.; Bree, G.; Ryan, K. M. Axial Si−Ge Heterostructure Nanowires as Lithium-Ion Battery Anodes. *Nano Lett.* **2018**, *18*, 5569−5575.
(53) Xiang, B.; An, W.-L.; Fu, J.-J.; Mei, S.-X.; Guo, S.-G.; Zhang, X.-M.; Gao, B.; Chu, P. K. Graphene-encapsulated blackberry-like porous silicon nanospheres prepared by modest magnesiothermic reduction for high-performance lithium-ion battery anode. *Rare Metals* **2021**, *40*, 383−392.
(54) An, W.; Gao, B.; Mei, S.; Xiang, B.; Fu, J.; Wang, L.; Zhang, Q.; Chu, P. K.; Huo, K. Scalable synthesis of ant-nest-like bulk porous silicon for high-performance lithium-ion battery anodes. *Nat. Commun.* **2019**, *10*, No. 1447.
(55) An, W.; Xiang, B.; Fu, J.; Mei, S.; Guo, S.; Huo, K.; Zhang, X.; Gao, B.; Chu, P. K. Three-dimensional carbon-coating silicon nanoparticles welded on carbon nanotubes composites for high-stability lithium-ion battery anodes. *Appl. Surf. Sci.* **2019**, *479*, 896−902.
(56) Weng, W.; Yang, J.; Zhou, J.; Gu, D.; Xiao, W. Template-Free Electrochemical Formation of Silicon Nanotubes from Silica. *Adv. Sci.* **2020**, *7*, No. 2001492.

https://doi.org/10.1021/acsaem.0c02932
ACS Appl. Energy Mater. XXXX, XXX, XXX−XXX